JOURNAL OF MOLECULAR SPECTROSCOPY 123, 145–160 (1987)

Study of the ν_3 and $2\nu_3 \leftarrow \nu_3$ Bands of $^{12}CH_3F$ by Infrared Laser Sideband and Submillimeter-Wave Spectroscopy[1]

SANG K. LEE[2] AND R. H. SCHWENDEMAN

Department of Chemistry, Michigan State University, East Lansing, Michigan 48824

AND

RICHARD L. CROWNOVER, DAVID D. SKATRUD,[3] AND FRANK C. DE LUCIA

Department of Physics, Duke University, Durham, North Carolina 27706

An infrared laser sideband spectrometer operating in the CO_2 laser region with 8- to 18-GHz sidebands has been used to record 266 transitions in the ν_3 band and 84 transitions in the $2\nu_3 \leftarrow \nu_3$ band of $^{12}CH_3F$. The accuracy of the measured frequencies is estimated to be 1–3 MHz. A millimeter/submillimeter-wave spectrometer has been used to record the spectra of 48 pure rotational transitions in the ground vibrational state and 55 transitions in the $v_3 = 1$ vibrational state with an accuracy of 20–90 kHz. The new measurements have been combined with previous radio frequency and infrared laser results to derive sets of constants for the ground, $v_3 = 1$, and $v_3 = 2$ states for this molecule. Tables of the vibrational dependence of the parameters and of the near coincidences of the ν_3 and $2\nu_3 \leftarrow \nu_3$ band transitions with CO_2 laser frequencies are given.

I. INTRODUCTION

Recently, portions of the ν_3 and $2\nu_3 \leftarrow \nu_3$ bands of $^{13}CH_3F$ were recorded at Michigan State University (MSU) by means of an infrared–microwave sideband laser spectrometer (*1*). In order to assign the weak hot-band transitions unambiguously, it proved necessary to measure the ν_3 spectrum of $^{12}CH_3F$, since the sample of $^{13}CH_3F$ used was not entirely free of the parent species. Because there have been a large number of recent high-resolution studies of the ν_3 band of $^{12}CH_3F$ (*2–5*), we expected to be able to calculate the frequencies to within 10–20 MHz with available constants, even for rather high J. It turned out, however, that for $J > 20$, particularly for P-branch transitions, the deviation between observed and calculated frequencies was rather sizeable, reaching more than 200 MHz (0.007 cm^{-1}).

Since the method of infrared–microwave sideband laser spectroscopy, as developed by Magerl and his co-workers (*6*) and applied to several spectroscopic studies (*1, 7–*

[1] This material is based on work partially supported at MSU by the National Science Foundation under Grant No. 83-12861 and at Duke University by the U.S. Army Research Office under Contract Nos. DAAG-29-83-K-0078 and DAAL-03-86-C-0011.

[2] Current address: Herzberg Institute of Astrophysics, National Research Council of Canada, Ottawa, Ontario K1A 0R6.

[3] Current address: Army Research Office, P.O. Box 12211, Research Triangle Park, NC 27709.

0022-2852/87 $3.00

15), can easily provide frequencies of spectra that are accurate to a few MHz, we decided to extend the study of the ν_3 band of $^{12}CH_3F$ to as many transitions as could be measured in the range of our spectrometer and also to record as much of the spectrum of the $2\nu_3 \leftarrow \nu_3$ band as possible. The analysis of the ν_3 band of $^{12}CH_3F$ has been discussed in detail many times (*2–5*) and the present analysis is very similar to the previous study of $^{13}CH_3F$ (*1*). We will therefore simply present the spectra and the resulting parameters and only briefly describe the experimental and theoretical details.

As part of a study at Duke University of the dynamics of far-infrared laser action in $^{12}CH_3F$ it was necessary to monitor the absorption of pure rotational transitions in the ground and $v_3 = 1$ vibrational states of this molecule. The millimeter-wave spectra of these transitions were at the time limited to relatively low J and K (*16–19*); therefore, the first step in this study was to measure the frequencies of a large number of rotational transitions in both vibrational states. Since these measurements were made, a report of millimeter- and submillimeter-wave frequencies for the ground vibrational state for the same J range and $K = 0, 3, 6$, etc., has appeared (*20*). Comparison of the results of these measurements with the values reported here is given below. In addition to the work already cited, rotation or vibration–rotation frequencies for the ground and $v_3 = 1$ states or for the ν_3 band have been measured by combination differences of Fourier transform spectra (*21*), IR-RF two-photon spectroscopy (*22*), diode laser spectroscopy (*23–24*), waveguide laser spectroscopy (*24*), and optical pumping (*25–28*).

In the present paper, Section II is a description of the experimental techniques used to record and measure the infrared, millimeter-wave, and submillimeter-wave frequencies. Section III describes the energy level expressions used to calculate the spectra, Section IV presents the results of least-squares fitting of the spectra, and Section V summarizes the results.

II. EXPERIMENTAL DETAILS

The infrared–microwave sideband laser spectrometer at MSU has been described in previous publications (*1, 14*) and therefore only a brief description will be given here. Infrared radiation (~0.5 W) from a frequency-stabilized CO_2 laser is focused onto a CdTe electrooptic crystal that is simultaneously irradiated by high-power (~10 W, 8–18 GHz) microwaves. The infrared carrier and microwave-generated sidebands are recollimated and passed through a polarizer that removes most of the carrier. The microwave radiation is chopped at 33.3 kHz by a PIN diode absorptive modulator before being applied to the sideband generator. For the present study, a feedback circuit controlled the amplitude of the applied microwaves during the "on" period of the PIN diode to maintain constant sideband power. With this system it is possible to sweep over 2–3 GHz (0.067–0.1 cm^{-1}) with the infrared amplitude at a reference detector held constant to within a few tenths of one percent. Figure 1 is a block diagram of the spectrometer showing the location of the leveling circuit and the PIN diode. The infrared sidebands are passed through a sample cell to a detector whose output is processed at 33.3 kHz by a lock-in amplifier. A minicomputer steps the microwave frequency and records the output of the lock-in amplifier that monitors the sample beam detector and the nearly constant output of a similar system for the reference beam.

The sample cells are simple glass tubes with NaCl windows. The path length was 1 m and the sample pressures, as measured by a capacitance manometer, were <200

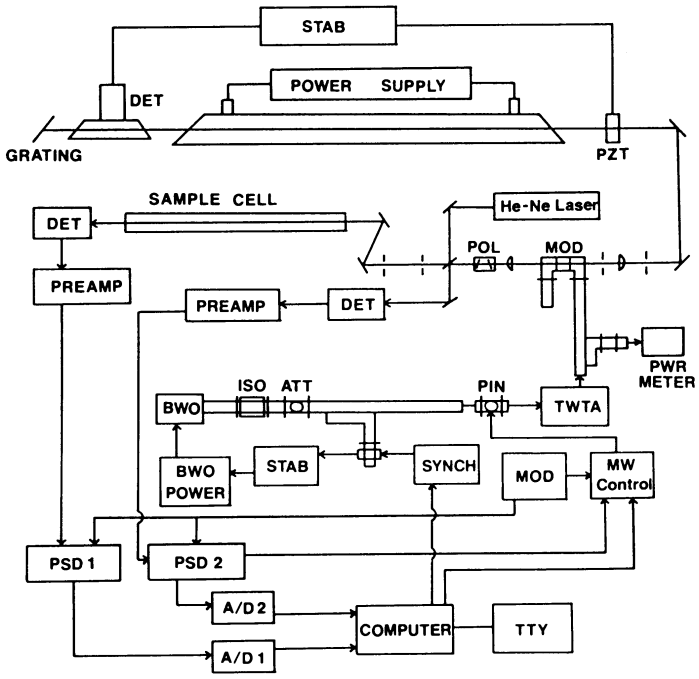

FIG. 1. Block diagram of the infrared laser microwave sideband spectrometer at MSU.

mTorr for the fundamental band and <1 Torr for the hot band. The $^{12}CH_3F$ sample used at MSU was obtained from Peninsular Chemical Research, Inc., and used as received. Composites of typical spectra are shown in Figs. 2 and 3. These spectra are

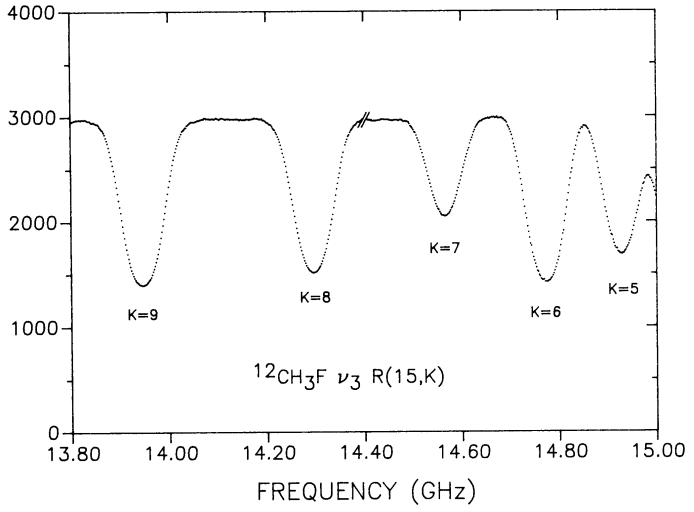

FIG. 2. Portion of the $R(15,K)$ spectrum in the ν_3 band of $^{12}CH_3F$ recorded with the infrared laser microwave sideband spectrometer. The horizontal axis shows the microwave frequency to be subtracted from the frequency of the $9R(12)$ CO_2 laser to obtain the spectrometer frequency. The spectrum shown is a composite of two recordings; the sample pressures were ~100 mTorr and ~50 mTorr for the left and right halves, respectively.

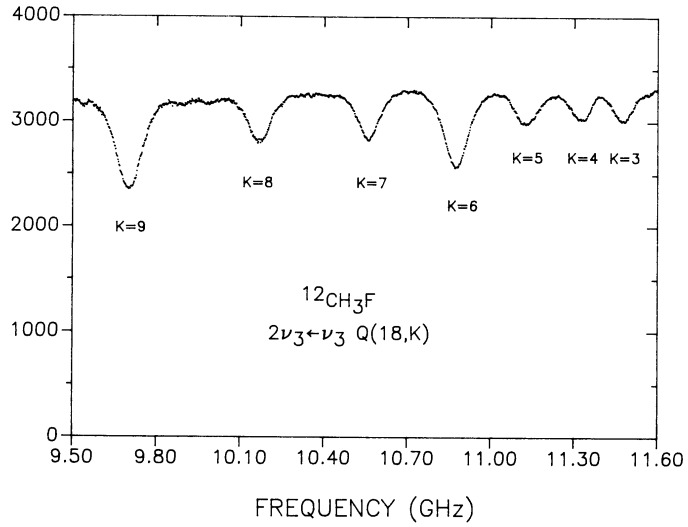

FIG. 3. Portion of the $Q(18,K)$ spectrum in the $2\nu_3 \leftarrow \nu_3$ band of $^{12}CH_3F$ recorded with the infrared laser microwave sideband spectrometer. The horizontal axis shows the microwave frequency to be subtracted from the frequency of the $9P(38)$ CO_2 laser to obtain the spectrometer frquency. The sample pressure was ~1 Torr.

reprinted as recorded from the spectrometer with no division by a reference spectrum. The flat background demonstrates the effectiveness of the amplitude-leveling system.

The recorded spectra were fit to a Gaussian lineshape as a function of microwave frequency. The infrared frequency of each transition was taken to be $\nu_l \pm \nu_m$, where ν_l is the known laser frequency and ν_m is the center frequency of the Gaussian function. Since the spectra were rather well characterized prior to this work, the proper sign was usually known. In questionable cases the usual spectrum recorded with the infrared laser stabilized to the Lamb dip in the fluorescence from an intracavity cell filled with CO_2 was compared to a spectrum recorded with the laser stabilized to one or another of the shoulders of the Lamb dip. The difference in the microwave frequencies of the two spectra provided an unambiguous choice of the sign in $\nu_l \pm \nu_m$. The overall accuracy of the individual spectral frequencies was estimated to be 1–3 MHz depending on the strength of the transition, the degree of overlapping, and the quality of the spectra in the given spectral region.

The pure rotational transitions were measured on a millimeter/submillimeter (mm/submm) wave spectrometer that has been developed at Duke University (*29*). This system provides continuous coverage from less than 100 GHz to greater than 1000 GHz with adequate sensitivity for room temperature absorption measurements in even highly excited vibrational states and transient species. Figure 4 shows a block diagram of the experimental apparatus. The mm/submm power is produced by a refined version of the crossed-waveguide crystal harmonic generator developed by King and Gordy (*30*). The multiplier is driven by an ~300-mW reflex klystron operating in the 55-GHz region. The output of the multiplier, after lower harmonics are removed by a waveguide-beyond-cutoff filter, is focused into a sample cell and then directed onto a 1.5 K InSb hot-electron bolometer. The sample cell is a copper pipe

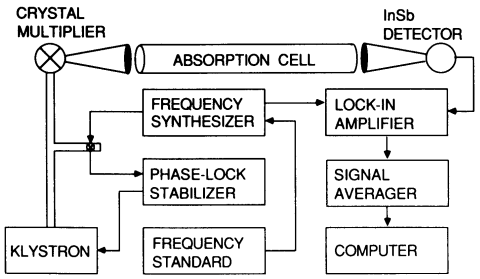

FIG. 4. Block diagram of the millimeter/submillimeter wave spectrometer at Duke University.

1 m in length by 1.25 cm in diameter. The klystron is phase-locked to a harmonic of a microprocessor-controlled frequency synthesizer capable of phase-continuous sweeps and simultaneous phase modulation. The data were typically acquired in segments that covered about 30 MHz with sweep times of 10 sec. The signal was phase-modulated at 1 kHz with lock-in detection at $2f$ and a time constant of 100 msec. Pairs of up/down frequency sweeps were averaged to cancel time-constant induced frequency shifts and other systematic errors. Additional signal enhancement was obtained by digitally signal averaging the individual frequency sweeps. The net integration time for the weakest signals was about 10 min.

The frequency synthesizer is locked to a frequency standard which is in turn referenced to WWVB. The frequency of the mm/submm waves is thus known to an absolute accuracy of better than 10^9 and since the multiplier is driven by a reflex klystron, the spectral purity is high. Therefore, the observed linewidths were entirely due to the widths of the rotational transitions themselves. The sample pressure was adjusted to be small enough so that the dominant line-broadening mechanism was Doppler broadening which for CH_3F has a HWHM of $\Delta\nu \simeq 10^{-6}\nu$. The typical pressure was ~30 mTorr, although lower pressures had to be used for many of the ground state transitions to prevent line broadening caused by near 100% absorption of the mm/submm wave power. The line centers were measured with an accuracy better than 5% of the HWHM by fitting a parabola to the peak of the absorptions. The 1σ uncertainty in the measurements was thus about 30 kHz (10^{-6} cm^{-1}) for transitions around 600 GHz.

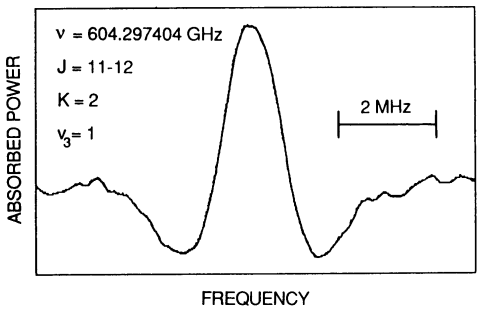

FIG. 5. The observed rotational absorption line for the $J = 12 \leftarrow 11$, $K = 2$ transition in the $v_3 = 1$ state of $^{12}CH_3F$. The sample pressure was ~35 mTorr and the total integration time was ~5 minutes.

TABLE I

Comparison of Observed and Calculated Frequencies in the ν_3 Band of $^{12}CH_3F$

Trans.	Laser[a]	ν_m[b]	ν/MHz	O-C[c]	Unc.[d]	ν/cm^{-1}[e]	Trans.	Laser[a]	ν_m[b]	ν/MHz	O-C[c]	Unc.[d]	ν/cm^{-1}[e]
P(30, 3)	10R(40)	10708.0	29618816.1	1.8	3.0	987.97736(6)	Q(29,14)	9P(28)	-17609.3	31141898.9	8.5	2.0	1038.78193(28)
P(30, 4)	10R(40)	10791.0	29618899.1	3.2	2.0	987.98013(10)	Q(29,15)	9P(28)	-17962.2	31141546.0	-7.0	2.0	1038.77016(-23)
P(30, 5)	10R(40)	10895.0	29619003.1	-0.6	2.0	987.98360(-1)	Q(26,14)	9P(26)	-16174.0	31200587.3	1.3	2.0	1040.73957(4)
P(30, 6)	10R(40)	11035.0	29619143.1	3.7	1.0	987.98827(12)	Q(26,15)	9P(26)	-15961.4	31200799.9	-3.2	1.0	1040.74666(-10)
P(30, 7)	10R(40)	11196.0	29619304.1	-0.3	2.0	987.99364(-1)	Q(21,11)	9P(24)	9628.6	31282875.8	1.9	2.0	1043.48442(6)
P(30, 8)	10R(40)	11396.6	29619504.7	4.7	1.0	988.00033(15)	Q(21,12)	9P(24)	10212.0	31283459.2	1.0	3.0	1043.50387(3)
P(30, 9)	10R(40)	11615.4	29619723.5	-3.1	1.0	988.00763(-10)	Q(21,13)	9P(24)	10934.1	31284181.3	6.1	2.0	1043.52796(20)
P(30,10)	10R(40)	11870.6	29619978.7	-5.6	1.0	988.01614(-18)	Q(21,14)	9P(24)	11809.8	31285057.0	1.5	2.0	1043.55717(5)
P(30,11)	10R(40)	12162.0	29620270.1	-2.5	2.0	988.02586(-8)	Q(21,15)	9P(24)	12890.2	31286137.3	-0.5	1.0	1043.59321(-1)
P(30,12)	10R(40)	12481.8	29620589.9	-0.5	1.0	988.03653(-1)	Q(21,16)	9P(24)	14215.0	31287462.2	-10.5	OMIT	1043.63740(-34)
							Q(21,18)	9P(24)	17926.2	31291173.3	-0.8	2.0	1043.76119(-2)
P(30,13)	10R(40)	12830.0	29620938.1	1.2	1.0	988.04814(3)	Q(19,11)	9P(22)	-17734.9	31311226.6	2.8	1.0	1044.43010(9)
P(30,14)	10R(40)	13209.9	29621318.1	5.9	2.0	988.06082(19)	Q(19,12)	9P(22)	-16965.5	31311996.0	-3.8	1.0	1044.45576(-12)
P(30,15)	10R(40)	13618.0	29621726.1	8.0	2.0	988.07443(26)	Q(19,13)	9P(22)	-16018.0	31312943.5	0.4	2.0	1044.48737(1)
P(29, 3)	10R(46)	-9418.8	29688610.5	-2.2	2.0	990.30545(-7)	Q(19,14)	9P(22)	-14870.7	31314090.8	0.1	1.0	1044.52564(0)
P(29, 4)	10R(46)	-9313.4	29688716.0	2.5	2.0	990.30897(8)	Q(19,15)	9P(22)	-13473.3	31315488.2	-1.4	1.0	1044.57225(-4)
P(29, 5)	10R(46)	-9182.0	29688847.3	1.0	2.0	990.31335(3)	Q(19,16)	9P(22)	-11765.1	31317196.4	-2.8	1.0	1044.62923(-9)
P(29, 6)	10R(46)	-9014.6	29689014.7	1.2	1.0	990.31893(3)	Q(19,17)	9P(22)	-9663.1	31319298.4	3.5	2.0	1044.69934(11)
P(29, 7)	10R(46)	-8813.6	29689215.7	-1.3	1.0	990.32564(-4)							
P(29, 8)	10R(46)	-8576.1	29689453.2	-5.7	2.0	990.33356(-19)	Q(17,13)	9P(22)	10017.4	31338978.9	3.1	2.0	1045.35581(10)
P(15, 2)	9P(46)	-10031.5	30600484.7	0.6	1.0	1020.72230(2)	Q(17,14)	9P(22)	11414.3	31340375.8	2.9	1.0	1045.40241(9)
							Q(17,15)	9P(22)	13111.6	31342073.1	6.4	3.0	1045.45903(21)
P(15, 3)	9P(46)	-9820.3	30600695.8	-1.0	1.0	1020.72934(-3)	Q(17,16)	9P(22)	15175.6	31344137.1	11.5	OMIT	1045.52787(38)
P(15, 4)	9P(46)	-9516.1	30601000.1	-0.9	1.0	1020.73949(-2)	Q(17,17)	9P(22)	17680.0	31346641.5	6.5	2.0	1045.61141(21)
P(15, 5)	9P(46)	-9113.1	30601403.1	0.5	1.0	1020.75293(1)	Q(16, 2)	9P(22)	15826.0	31344787.5	0.4	2.0	1045.54957(1)
P(15, 6)	9P(46)	-8604.5	30601911.6	1.3	2.0	1020.76990(4)	Q(16, 3)	9P(22)	15955.1	31344916.6	5.3	2.0	1045.55388(17)
P(14, 2)	9P(44)	-13593.9	30660851.9	-2.9	1.0	1022.73593(-9)	Q(16, 4)	9P(22)	16130.0	31345091.5	0.5	2.0	1045.55971(1)
P(14, 3)	9P(44)	-13374.0	30661071.7	-2.0	1.0	1022.74326(-6)	Q(16, 5)	9P(22)	16372.0	31345333.5	1.7	1.0	1045.56778(5)
P(14, 4)	9P(44)	-13059.9	30661385.8	-0.7	1.0	1022.75374(-2)	Q(16, 6)	9P(22)	16682.1	31345643.6	2.0	1.0	1045.57812(6)
P(14, 5)	9P(44)	-12647.9	30661797.9	-2.0	1.0	1022.76749(-6)							
P(14, 6)	9P(44)	-12124.6	30662321.2	-1.3	1.0	1022.78494(-4)	Q(16, 7)	9P(22)	17069.2	31346030.7	0.7	1.0	1045.59104(2)
P(14, 7)	9P(44)	-11480.8	30662964.9	-1.0	1.0	1022.80642(-3)	Q(16, 8)	9P(22)	17550.2	31346511.7	2.0	2.0	1045.60708(6)
							Q(14, 4)	9P(20)	-17839.5	31366060.9	-0.9	1.0	1046.25917(-2)
P(14, 8)	9P(44)	-10701.3	30663744.5	0.1	1.0	1022.83242(0)	Q(14, 5)	9P(20)	-17556.8	31366343.6	-1.5	1.0	1046.26860(-5)
P(14, 9)	9P(44)	-9769.6	30664676.1	0.5	1.0	1022.86350(1)	Q(14, 6)	9P(20)	-17192.8	31366707.6	-0.8	1.0	1046.28075(-2)
P(14,10)	9P(44)	-8664.0	30665781.8	-0.2	2.0	1022.90038(0)	Q(14, 7)	9P(20)	-16738.0	31367162.4	-0.2	2.0	1046.29591(0)
P(13, 2)	9P(42)	-17079.2	30720577.5	2.3	1.0	1024.72816(7)	Q(14, 8)	9P(20)	-16179.6	31367720.8	-0.5	1.0	1046.31454(-1)
P(13, 3)	9P(42)	-16857.8	30720798.9	-0.5	1.0	1024.73555(-1)	Q(14, 9)	9P(20)	-15495.0	31368405.4	3.6	2.0	1046.33738(12)
P(13, 4)	9P(42)	-16537.2	30721119.5	-0.6	1.0	1024.74624(-1)	Q(14,10)	9P(20)	-14676.7	31369223.7	-1.6	1.0	1046.36467(-5)
P(13, 5)	9P(42)	-16112.8	30721543.9	0.0	1.0	1024.76040(0)	Q(14,11)	9P(20)	-13681.7	31370218.7	0.7	1.0	1046.39786(2)
P(13, 6)	9P(42)	-15576.7	30722080.0	-0.1	1.0	1024.77828(0)							
P(13, 7)	9P(42)	-14916.5	30722740.2	-0.3	1.0	1024.80030(0)	Q(14,12)	9P(20)	-12490.2	31371410.2	-3.0	1.0	1046.43760(-9)
P(13, 8)	9P(42)	-14117.0	30723539.8	-0.2	1.0	1024.82697(0)	Q(14,13)	9P(20)	-11049.5	31372850.9	-0.5	1.0	1046.48566(-1)
							Q(14,14)	9P(20)	-9313.0	31374587.4	3.7	3.0	1046.54359(12)
P(13, 9)	9P(42)	-13159.7	30724497.0	-0.3	1.0	1024.85890(0)	Q(13, 2)	9P(20)	-8745.1	31375155.3	-1.4	2.0	1046.56253(-4)
P(13,10)	9P(42)	-12022.8	30725633.9	-1.6	1.0	1024.89683(-5)	Q(13, 3)	9P(20)	-8587.9	31375312.5	-1.6	1.0	1046.56777(-5)
P(13,11)	9P(42)	-10675.0	30726981.7	-1.9	1.0	1024.94178(-6)	Q(13, 4)	9P(20)	-8361.4	31375539.0	-2.0	1.0	1046.57533(-6)
P(13,12)	9P(42)	-9078.1	30728578.6	1.3	1.0	1024.99505(4)	Q(11, 7)	9P(20)	9896.4	31393796.8	5.0	1.0	1047.18434(16)
P(12, 8)	9P(40)	-17469.1	30782673.6	-0.4	1.0	1026.79947(-1)	Q(11, 8)	9P(20)	10555.4	31394455.8	2.9	1.0	1047.20633(9)
P(12, 9)	9P(40)	-16488.2	30783654.5	0.0	1.0	1026.83219(0)	Q(11, 9)	9P(20)	11356.9	31395257.3	1.7	1.0	1047.23306(5)
P(12,10)	9P(40)	-15321.5	30784821.2	-0.2	1.0	1026.87110(0)	Q(11,11)	9P(20)	13489.0	31397389.4	1.0	1.0	1047.30418(3)
P(12,11)	9P(40)	-13940.6	30786202.1	-2.5	1.0	1026.91716(-8)							
P(5, 2)	9P(28)	15136.0	31174644.2	0.7	1.0	1039.87420(2)	Q(10, 2)	9P(20)	15591.1	31399491.5	0.7	2.0	1047.37430(2)
P(5, 3)	9P(28)	15378.8	31174887.0	1.6	1.0	1039.88230(5)	Q(10, 3)	9P(20)	15776.3	31399676.7	1.1	1.0	1047.38048(3)
							Q(10, 4)	9P(20)	16042.3	31399942.7	1.2	1.0	1047.38935(4)
P(5, 4)	9P(28)	15724.3	31175232.4	0.4	2.0	1039.89382(1)	Q(10, 5)	9P(20)	16396.6	31400297.0	1.3	1.0	1047.40117(4)
P(4, 2)	9P(26)	11648.0	31228409.3	1.0	1.0	1041.66761(3)	Q(10, 6)	9P(20)	16849.1	31400749.5	1.4	2.0	1047.41626(4)
P(4, 3)	9P(26)	11889.3	31228650.6	1.5	1.0	1041.67566(5)	Q(10, 7)	9P(20)	17412.6	31401313.0	1.5	1.0	1047.43506(5)
Q(39,12)	9P(36)	-15133.5	30907781.9	1.5	2.0	1030.97263(5)	Q(6, 1)	9P(18)	-15679.2	31422381.0	0.7	2.0	1048.13781(2)
Q(38, 9)	9P(36)	14669.9	30937585.3	2.3	2.0	1031.96676(7)	Q(6, 2)	9P(18)	-15555.1	31422505.1	0.2	1.0	1048.14195(0)
Q(33, 3)	9P(32)	17624.0	31060342.1	-12.5	OMIT	1036.06149(-41)	Q(6, 3)	9P(18)	-15344.0	31422716.2	0.0	1.0	1048.14899(0)
Q(33, 4)	9P(32)	17420.0	31060138.1	-9.7	3.0	1036.05469(-32)	Q(6, 4)	9P(18)	-15041.2	31423019.0	-0.7	1.0	1048.15909(-2)
Q(33, 5)	9P(32)	17158.0	31059876.1	-7.3	2.0	1036.04595(-24)							
Q(33, 6)	9P(32)	16839.1	31059557.2	-4.4	1.0	1036.03531(-14)	Q(6, 5)	9P(18)	-14637.5	31423422.7	-0.8	1.0	1048.17256(-2)
Q(33, 7)	9P(32)	16470.6	31059188.6	6.8	2.0	1036.02302(22)	Q(6, 6)	9P(18)	-14121.0	31423939.2	0.7	1.0	1048.18979(2)
							Q(5, 2)	9P(18)	-11491.8	31426568.3	-1.1	1.0	1048.27748(-3)
Q(33, 8)	9P(32)	16029.2	31058747.3	5.1	1.0	1036.00829(16)	Q(5, 3)	9P(18)	-11275.8	31426784.3	-1.1	1.0	1048.28469(-3)
Q(33, 9)	9P(32)	15523.3	31058241.4	2.4	1.0	1035.99142(7)	Q(5, 4)	9P(18)	-10965.1	31427095.1	-0.6	1.0	1048.29506(-1)
Q(33,10)	9P(32)	14946.5	31057664.6	-1.9	1.0	1035.97218(-6)	Q(5, 5)	9P(18)	-10552.0	31427508.2	-0.2	1.0	1048.30883(0)
Q(33,11)	9P(32)	14297.3	31057015.4	-0.7	1.0	1035.95052(-2)	R(2, 2)	9P(12)	-9962.1	31585869.7	1.8	2.0	1053.59120(6)
Q(33,12)	9P(32)	13555.4	31056273.5	-3.6	1.0	1035.92578(-11)	R(3, 2)	9P(10)	-12623.9	31634219.5	2.5	1.0	1055.20398(8)
Q(33,13)	9P(32)	12711.8	31055429.9	-5.8	2.0	1035.89764(-19)	R(3, 3)	9P(10)	-12424.0	31634419.4	0.0	1.0	1055.21065(0)
Q(29, 8)	9P(28)	-16017.2	31143491.0	0.9	2.0	1038.83504(2)	R(4, 2)	9P(8)	-15175.5	31681885.9	2.7	2.0	1056.79396(8)
Q(29, 9)	9P(28)	-16236.6	31143271.6	-3.2	1.0	1038.82772(-10)							
Q(29,10)	9P(28)	-16478.0	31143030.2	-9.3	OMIT	1038.81967(-31)	R(4, 3)	9P(8)	-14985.5	31682075.9	-1.3	1.0	1056.80030(-4)
Q(29,11)	9P(28)	-16721.7	31142786.4	2.5	2.0	1038.81154(8)	R(4, 4)	9P(8)	-14705.3	31682356.1	-0.7	1.0	1056.80965(-2)
							R(5, 2)	9P(6)	-17620.0	31728863.8	-1.7	2.0	1058.36097(-5)
Q(29,12)	9P(28)	-17001.8	31142506.4	-1.0	2.0	1038.80220(-3)	R(5, 3)	9P(6)	-17433.9	31729049.9	-0.6	1.0	1058.36718(-1)
Q(29,13)	9P(28)	-17293.0	31142215.1	5.7	1.0	1038.79248(19)	R(5, 4)	9P(6)	-17167.8	31729316.0	-1.1	1.0	1058.37606(-3)

[a] CO_2 laser line used.

[b] Microwave frequency in MHz. The signed microwave frequency is added to the laser frequency to obtain the absorption frequency.

[c] Observed minus calculated frequency in MHz. The parameters for the calculation are in the second and third columns of Table VI.

[d] Estimated uncertainty in the observed frequency in MHz. An "OMIT" means that the frequency was omitted from the least squares fits.

[e] Observed frequency in cm^{-1}. The numbers in parentheses are the observed minus calculated frequencies in units of 0.00001 cm^{-1}.

TABLE I—*Continued*

Trans.	Laser[a]	ν_m[b]	ν/MHz	O-C[c]	Unc.[d]	ν/cm^{-1} [e]	Trans.	Laser[a]	ν_m[b]	ν/MHz	O-C[c]	Unc.[d]	ν/cm^{-1} [e]
R(5, 5)	9P(6)	-16809.9	31729673.9	0.3	1.0	1058.38800(1)	R(16,11)	9R(14)	-14972.5	32202118.7	0.3	1.0	1074.14706(0)
R(13, 3)	9R(8)	-11563.0	32080089.7	-0.5	2.0	1070.07661(-1)	R(16,12)	9R(14)	-14356.7	32202734.6	-0.1	1.0	1074.16760(0)
R(13, 4)	9R(8)	-11436.0	32080216.7	0.4	1.0	1070.08084(1)	R(16,13)	9R(14)	-13567.1	32203524.2	2.2	1.0	1074.19394(7)
R(13, 5)	9R(8)	-11263.0	32080389.6	0.3	1.0	1070.08661(1)	R(16,14)	9R(14)	-12568.3	32204523.0	-0.8	1.0	1074.22726(-2)
R(13, 6)	9R(8)	-11034.8	32080617.9	0.0	1.0	1070.09423(0)	R(16,15)	9R(14)	-11300.7	32205790.6	-3.7	1.0	1074.26954(-12)
							R(17, 7)	9R(16)	-17972.4	32239330.9	-0.2	1.0	1075.38832(0)
R(13, 7)	9R(8)	-10740.4	32080912.3	-0.7	1.0	1070.10405(-2)	R(17, 8)	9R(16)	-17816.7	32239486.7	-1.5	1.0	1075.39352(-5)
R(13, 8)	9R(8)	-10364.1	32081288.6	0.3	1.0	1070.11660(0)	R(17, 9)	9R(16)	-17601.5	32239701.8	-2.2	1.0	1075.40070(-7)
R(13, 9)	9R(8)	-9890.8	32081761.9	0.5	1.0	1070.13239(1)	R(17,10)	9R(16)	-17310.4	32239993.0	-2.3	1.0	1075.41041(-7)
R(13,10)	9R(8)	-9298.9	32082353.7	0.3	2.0	1070.15213(0)	R(17,11)	9R(16)	-16922.0	32240381.3	-1.1	1.0	1075.42336(-3)
R(13,11)	9R(8)	-8559.2	32083093.5	2.5	3.0	1070.17680(8)							
R(14, 3)	9R(10)	-13400.0	32120866.9	-1.0	3.0	1071.43679(-3)	R(17,12)	9R(16)	-16412.8	32240890.6	-0.6	1.0	1075.44035(-1)
R(14, 4)	9R(10)	-13294.8	32120972.2	0.1	2.0	1071.44030(0)	R(17,13)	9R(16)	-15736.3	32241567.0	13.5	OMIT	1075.46291(45)
R(14, 5)	9R(10)	-13150.0	32121116.9	0.3	1.0	1071.44513(1)	R(17,14)	9R(16)	-14890.8	32242412.6	2.8	1.0	1075.49112(9)
R(14, 6)	9R(10)	-12958.5	32121308.4	-1.1	1.0	1071.45152(-3)	R(17,15)	9R(16)	-13796.5	32243506.9	-3.9	2.0	1075.52762(-13)
R(14, 7)	9R(10)	-12706.5	32121560.4	-0.8	1.0	1071.45992(-2)	R(18,13)	9R(18)	-17838.0	32278879.0	6.4	2.0	1076.70751(21)
							R(18,14)	9R(18)	-17141.3	32279575.7	-2.9	1.0	1076.73075(-9)
R(14, 9)	9R(10)	-11965.6	32122301.3	3.9	1.0	1071.48464(13)	R(18,15)	9R(18)	-16208.3	32280508.9	4.3	2.0	1076.76187(14)
R(14,10)	9R(10)	-11447.3	32122819.6	1.2	1.0	1071.50192(3)	R(22, 3)	9R(24)	12028.0	32422213.7	-1.5	2.0	1081.48864(-5)
R(14,11)	9R(10)	-10792.1	32123474.8	1.5	1.0	1071.52378(5)	R(22, 4)	9R(24)	11931.0	32422116.7	0.7	2.0	1081.48540(2)
R(14,12)	9R(10)	-9973.3	32124293.6	0.2	1.0	1071.55109(0)	R(22, 5)	9R(24)	11808.0	32421993.7	-1.1	2.0	1081.48130(-3)
R(15, 4)	9R(12)	-15044.0	32161035.5	-0.9	2.0	1072.77667(-3)							
R(15, 5)	9R(12)	-14929.6	32161149.9	-1.2	1.0	1072.78049(-3)	R(22, 6)	9R(24)	11670.0	32421855.7	-0.4	2.0	1081.47670(-1)
R(15, 6)	9R(12)	-14773.7	32161305.8	-1.1	1.0	1072.78569(-3)	R(22, 7)	9R(24)	11522.0	32421707.7	1.9	2.0	1081.47176(6)
R(15, 7)	9R(12)	-14567.6	32161511.9	-1.8	1.0	1072.79256(-5)	R(22, 8)	9R(24)	11366.0	32421551.7	1.3	2.0	1081.46656(4)
R(15, 8)	9R(12)	-14296.3	32161783.1	-0.7	1.0	1072.80161(-2)	R(22, 9)	9R(24)	11214.0	32421399.7	1.5	2.0	1081.46149(4)
R(15, 9)	9R(12)	-13947.0	32162132.5	-0.4	1.0	1072.81326(-1)	R(22,10)	9R(24)	11074.0	32421259.7	0.9	2.0	1081.45682(2)
							R(23, 3)	9R(26)	10350.0	32456775.0	0.2	2.0	1082.64148(0)
R(15,10)	9R(12)	-13499.3	32162580.2	0.1	1.0	1072.82819(0)	R(23, 4)	9R(26)	10222.1	32456647.1	0.0	1.0	1082.63721(0)
R(15,11)	9R(12)	-12930.1	32163149.4	0.4	1.0	1072.84718(1)	R(23, 5)	9R(26)	10067.7	32456492.6	4.0	1.0	1082.63206(13)
R(15,13)	9R(12)	-11301.6	32164777.9	0.8	1.0	1072.90150(2)	R(23, 6)	9R(26)	9880.0	32456304.9	1.2	1.0	1082.62580(4)
R(15,14)	9R(12)	-10154.0	32165925.5	6.3	2.0	1072.93978(20)	R(23, 7)	9R(26)	9673.7	32456098.6	1.4	1.0	1082.61892(4)
R(16, 5)	9R(14)	-16601.5	32200489.8	-3.1	2.0	1074.09272(-10)							
R(16, 6)	9R(14)	-16482.1	32200609.2	-1.0	1.0	1074.09671(-3)	R(23, 8)	9R(26)	9450.6	32455875.6	0.6	1.0	1082.61148(1)
R(16, 7)	9R(14)	-16321.7	32200769.6	-0.7	1.0	1074.10206(-2)	R(23, 9)	9R(26)	9222.7	32455647.6	3.4	1.0	1082.60387(11)
R(16, 8)	9R(14)	-16108.1	32200983.2	-1.7	1.0	1074.10918(-5)							
R(16, 9)	9R(14)	-15824.3	32201266.9	-1.5	1.0	1074.11865(-4)							
R(16,10)	9R(14)	-15453.3	32201638.0	-0.9	1.0	1074.13102(-3)							

The CH_3F sample used at Duke was obtained from Matheson Gas products. Figure 5 shows a typical absorption line, in this case the $J = 12 \leftarrow 11$, $K = 2$ transition in the $\nu_3 = 1$ vibrational state. This is the strongest lasing transition in the CH_3F optically pumped far-infrared laser (*31*). Although the absorptivities of the rotational transitions in the excited vibrational state are ~150 times smaller than in the ground state, a strong signal is still obtained with a reasonable integration time because of the large rotational absorption coefficients at these frequencies and the sensitivity of the system.

III. THEORY

The spectral frequencies were fit to differences in energy levels given by the following expression,

$$E(v,J,K) = \sum_{m,n=0}^{m+n=N} X_{mn}^{(v)} f^m g^n, \tag{1}$$

where $f = J(J+1)$, $g = K^2$, and the $X_{mn}^{(v)}$ are the usual vibration–rotation constants:

$$X_{00}^{(v)} = \text{vibrational energy}, \qquad X_{10}^{(v)} = B_v, \qquad X_{01}^{(v)} = (A_v - B_v),$$

$$X_{20}^{(v)} = -D_J^{(v)}, \qquad X_{11}^{(v)} = -D_{JK}^{(v)}, \qquad X_{02}^{(v)} = -D_K^{(v)},$$

$$X_{30}^{(v)} = H_J, \qquad X_{40}^{(v)} = L_J, \qquad \text{etc.}$$

Since very good ground state constants were available from the work of Graner (*21*), Arimondo *et al.* (*5*), and Boucher *et al.* (*20*), we extended our program to allow simultaneous fitting of the rotational frequencies in any level and of the frequencies of the fundamental and the hot band to obtain constants for $\nu_3 = 0$, 1, and 2 all at once,

TABLE II

Comparison of Observed and Calculated Frequencies in the $2\nu_3 \leftarrow \nu_3$ Band of $^{12}CH_3F$

Trans.	Laser[a]	ν_m[b]	ν/MHz	O-C[c]	Unc.[d]	ν/cm^{-1} [e]	Trans.	Laser[a]	ν_m[b]	ν/MHz	O-C[c]	Unc.[d]	ν/cm^{-1} [e]
R(17,12)	9P(6)	10835.0	31757318.8	-0.7	2.0	1059.31013(-2)	Q(16, 9)	9P(38)	13358.2	30875255.7	0.5	1.0	1029.88767(1)
R(15, 9)	9P(8)	-17765.0	31679296.4	-3.7	2.0	1056.70758(-12)	Q(16, 8)	9P(38)	12825.7	30874723.2	3.6	1.0	1029.86991(11)
R(12,10)	9P(14)	14935.0	31558963.9	-1.5	3.0	1052.69372(-5)	Q(16, 6)	9P(38)	12020.0	30873917.5	3.5	2.0	1029.84304(11)
R(12, 9)	9P(14)	14453.4	31558482.3	1.7	2.0	1052.67766(5)							
R(12, 8)	9P(14)	14057.9	31558086.8	-2.2	2.0	1052.66447(-7)	Q(13,13)	9P(36)	-14028.6	30908886.8	0.0	1.0	1031.00949(0)
R(12, 7)	9P(14)	13749.0	31557777.9	2.7	1.0	1052.65416(8)	Q(13,12)	9P(36)	-15278.9	30907636.6	-1.2	2.0	1030.96778(-4)
R(12, 6)	9P(14)	13494.9	31557523.8	-2.6	1.0	1052.64569(-8)	Q(13,10)	9P(36)	-17224.0	30905691.4	0.7	2.0	1030.90290(2)
R(12, 5)	9P(14)	13303.7	31557332.6	0.5	1.0	1052.63931(1)	Q(13, 9)	9P(36)	-17973.4	30904942.0	-0.6	2.0	1030.87790(-1)
R(12, 4)	9P(14)	13152.0	31557180.9	-2.8	2.0	1052.63425(-9)	Q(12,10)	9P(36)	-8605.5	30914310.0	1.2	2.0	1031.19038(4)
R(12, 3)	9P(14)	13045.0	31557073.9	-0.9	3.0	1052.63068(-2)	Q(12, 9)	9P(36)	-9388.1	30913527.4	-1.4	1.0	1031.16428(-4)
							Q(12, 8)	9P(36)	-10040.4	30912875.1	-1.6	1.0	1031.14252(-5)
R(10,10)	9P(16)	-16282.7	31475154.7	-1.8	2.0	1049.89815(-6)	Q(12, 7)	9P(36)	-10579.0	30912336.4	0.7	3.0	1031.12455(2)
R(10, 9)	9P(16)	-16866.1	31474571.3	1.4	1.0	1049.87869(4)	Q(12, 6)	9P(36)	-11022.0	30911893.4	1.4	3.0	1031.10978(4)
R(10, 8)	9P(16)	-17349.9	31474087.5	-3.0	2.0	1049.86255(-9)	Q(12, 5)	9P(36)	-11329.0	30911536.6	2.4	3.0	1031.09787(8)
R(10, 7)	9P(16)	-17737.1	31473700.3	-1.3	1.0	1049.84964(-4)							
R(9, 3)	9P(18)	-8380.0	31429680.2	-1.9	3.0	1048.38128(-6)	Q(12, 4)	9P(36)	-11660.0	30911255.4	2.5	3.0	1031.08849(8)
R(9, 2)	9P(18)	-8488.0	31429572.2	-2.3	2.0	1048.37768(-7)	Q(12, 3)	9P(36)	-11874.0	30911041.4	0.3	1.0	1031.08136(0)
R(7, 6)	9P(22)	13218.7	31342180.2	0.6	2.0	1045.46260(2)	Q(9, 9)	9P(36)	12434.1	30935349.5	0.8	1.0	1031.89219(2)
R(7, 5)	9P(22)	12899.9	31341861.4	0.1	2.0	1045.45196(0)	Q(9, 8)	9P(36)	11710.0	30934625.4	0.9	3.0	1031.86803(2)
R(7, 4)	9P(22)	12651.7	31341613.2	-0.6	1.0	1045.44368(-2)	Q(9, 7)	9P(36)	11110.0	30934025.4	2.3	3.0	1031.84802(7)
R(7, 3)	9P(22)	12463.7	31341425.2	-3.8	1.0	1045.43742(-12)	Q(9, 6)	9P(36)	10614.0	30933529.4	0.0	3.0	1031.83148(0)
							Q(9, 5)	9P(36)	10218.0	30933133.4	2.5	2.0	1031.81827(8)
R(4, 4)	9P(26)	-12455.9	31204305.4	0.1	1.0	1040.86359(0)	Q(9, 4)	9P(36)	9903.1	30932818.5	0.8	2.0	1031.80776(2)
R(4, 3)	9P(26)	-12677.7	31204083.6	1.4	1.0	1040.85619(4)	Q(9, 3)	9P(36)	9668.0	30932583.4	1.7	3.0	1031.79992(5)
R(4, 2)	9P(26)	-12835.0	31203926.3	-0.8	2.0	1040.85094(-2)	Q(8, 8)	9P(36)	17647.0	30940562.5	0.6	3.0	1032.06607(2)
Q(23,12)	9P(40)	-15667.8	30784474.9	0.0	1.0	1026.85955(0)							
Q(23, 9)	9P(40)	-16924.0	30783218.6	-0.7	2.0	1026.81765(-2)	Q(8, 7)	9P(36)	17026.6	30939942.1	-1.1	2.0	1032.04538(-3)
Q(21, 9)	9P(40)	12598.8	30812741.5	3.5	2.0	1027.80242(11)	Q(8, 6)	9P(36)	16521.4	30939436.8	1.6	1.0	1032.02852(5)
Q(18,10)	9P(38)	-9140.0	30852757.5	-4.9	3.0	1029.13721(-16)	Q(8, 5)	9P(36)	16112.0	30939027.5	2.4	1.0	1032.01487(7)
Q(18, 9)	9P(38)	-9701.4	30852196.1	-1.2	1.0	1029.11849(-3)	Q(8, 4)	9P(36)	15785.5	30938701.0	-1.7	1.0	1032.00398(-5)
Q(18, 8)	9P(38)	-10169.1	30851728.4	0.4	1.0	1029.10289(1)	Q(8, 3)	9P(36)	15547.4	30938462.9	3.0	1.0	1031.99604(10)
Q(18, 7)	9P(38)	-10557.5	30851340.1	-0.9	1.0	1029.08993(-3)	Q(8, 2)	9P(36)	15378.2	30938293.6	3.0	3.0	1031.99039(10)
							P(1, 0)	9P(36)	-11660.0	30911255.4	-1.7	3.0	1031.08849(-5)
Q(18, 6)	9P(38)	-10875.0	30851022.5	-2.5	1.0	1029.07934(-8)	P(7, 6)	9P(46)	-13658.6	30596857.6	-0.7	1.0	1020.60131(-2)
Q(18, 5)	9P(38)	-11125.2	30850772.3	1.2	1.0	1029.07099(3)	P(7, 5)	9P(46)	-14171.0	30596345.2	-2.6	1.0	1020.58422(-8)
Q(18, 4)	9P(38)	-11325.0	30850572.5	0.3	1.0	1029.06433(1)	P(7, 4)	9P(46)	-14570.0	30595946.1	2.1	2.0	1020.57091(6)
Q(18, 3)	9P(38)	-11475.0	30850422.5	-0.2	2.0	1029.05933(0)							
Q(16,12)	9P(38)	15683.1	30877580.6	0.3	1.0	1029.96522(1)	P(7, 3)	9P(46)	-14877.0	30595639.1	0.6	1.0	1020.56067(1)
Q(16,11)	9P(38)	14769.6	30876667.1	0.9	1.0	1029.93475(2)	P(7, 2)	9P(46)	-15090.7	30595425.5	0.7	1.0	1020.55354(2)
Q(16,10)	9P(38)	13998.0	30875895.5	-2.7	2.0	1029.90902(-9)							

[a] CO_2 laser line used.

[b] Microwave frequency in MHz. The signed microwave frequency is added to the laser frequency to obtain the absorption frequency.

[c] Observed minus calculated frequency in MHz. The parameters for the calculation are in the third and fourth columns of Table VI.

[d] Estimated uncertainty in the observed frequency in MHz.

[e] Observed frequency in cm^{-1}. The numbers in parentheses are the observed minus calculated frequencies in units of 0.00001 cm^{-1}.

or to obtain constants with the $v = 0$ values constrained. In all of the least-squares fittings the weight assigned to each experimental frequency was σ^{-2} where σ is the uncertainty in the measured value.

Since vibration–rotation parameters have been determined in this work for the $v_3 = 0$, 1, and 2 vibrational levels of $^{12}CH_3F$, it is possible to estimate the first three constants in an expansion of these parameters in powers of v_3. We used an expression of the form,

$$P(v) = P(0) + c_1 v + c_2 v^2, \tag{2}$$

where $P(v)$ is a parameter for the vibrational level v and c_1 and c_2 are constants.

The rotational levels of the $v_3 = 1$ (and presumably $v_3 = 2$) state of CH_3F are involved in a mild Coriolis resonance with the $v_6 = 1$ (and higher) levels. This resonance was ignored in the present work and the effects of the resonance are therefore included in the values of the parameters. The magnitude of these effects, which are substantial, has been estimated (*4*). In Ref. (*4*) it was shown that the standard deviation in the fit

TABLE III

Comparison of Observed and Calculated Rotational Frequencies in the $\nu_3 = 0$ Vibrational State of $^{12}CH_3F$

Trans.	ν/MHz	O-C[a]	Unc.[b]	ν/cm^{-1} [c]
R(4, 0)	255331.372	-0.010	0.03	8.5169378
R(4, 1)	255326.975	-0.012	0.03	8.5167911
R(4, 2)	255313.776	-0.030	0.03	8.5163509
R(4, 3)	255291.813	-0.033	0.03	8.5156183
R(4, 4)	255261.107	-0.012	0.03	8.5145940
R(5, 0)	306381.753	-0.003	0.03	10.2197952
R(5, 2)	306360.656	-0.011	0.03	10.2190915
R(5, 3)	306334.304	-0.013	0.03	10.2182125
R(5, 4)	306297.441	-0.008	0.03	10.2169829
R(5, 5)	306250.069	-0.015	0.03	10.2154027
R(7, 0)	408455.034	0.003	0.04	13.6245934
R(7, 1)	408447.990	-0.017	0.04	13.6243584
R(7, 2)	408426.944	0.020	0.04	13.6236564
R(7, 5)	408279.509	-0.004	0.04	13.6187385
R(7, 7)	408111.375	-0.044	0.04	13.6131302
R(8, 0)	459475.072	0.021	0.05	15.3264387
R(8, 3)	459403.913	-0.004	0.05	15.3240651
R(8, 8)	458970.576	-0.010	0.05	15.3096105
R(9, 0)	510482.062	0.010	0.05	17.0278487
R(10, 0)	561474.583	-0.013	0.06	18.7287761
R(10, 1)	561464.906	-0.029	0.06	18.7284533
R(10, 3)	561387.662	-0.021	0.06	18.7258768
R(10, 7)	561002.266	-0.070	0.06	18.7130213
R(10,10)	560513.161	-0.071	0.06	18.6967065
R(12, 0)	663410.586	0.065	0.07	22.1289952
R(12, 1)	663399.088	-0.020	0.07	22.1286117
R(12, 2)	663364.905	0.030	0.07	22.1274714
R(12, 3)	663307.859	0.015	0.07	22.1255686
R(12, 4)	663228.026	-0.022	0.07	22.1229056
R(12, 5)	663125.561	0.027	0.07	22.1194878
R(12, 6)	663000.388	0.025	0.07	22.1153125
R(12, 7)	662852.641	0.031	0.07	22.1103841
R(12, 9)	662489.734	0.014	0.07	22.0982789
R(12,10)	662274.815	0.014	0.07	22.0911099
R(12,11)	662037.693	-0.038	0.07	22.0832004
R(12,12)	661778.656	0.003	0.07	22.0745599
R(14, 0)	765271.271	0.020	0.08	25.5267019
R(14, 1)	765258.126	0.038	0.08	25.5262634
R(14, 3)	765152.858	0.026	0.08	25.5227521
R(14, 6)	764798.246	0.041	0.08	25.5109235
R(14, 9)	764209.295	0.029	0.08	25.4912782
R(14,12)	763389.225	0.050	0.08	25.4639236
R(14,14)	762716.190	0.028	0.08	25.4414736
R(15, 0)	816169.798	-0.003	0.08	27.2244940
R(15, 3)	816043.546	0.028	0.08	27.2202827
R(16, 0)	867045.141	-0.070	0.09	28.9215128
R(16, 6)	866509.404	0.038	0.09	28.9036425
R(16, 9)	865842.315	0.070	0.09	28.8813908

[a] Observed minus calculated frequency in MHz. The parameters for the calculation are in the $v_3 = 0$ column of Table VI.

[b] Estimated uncertainty in the observed frequency in MHz.

[c] Observed frequency in cm^{-1}.

TABLE IV

Comparison of Observed and Calculated Rotational Frequencies in the $v_3 = 1$ Vibrational State of $^{12}CH_3F$

Trans.	ν/MHz	O-C[a]	Unc.[b]	ν/cm^{-1} [c]
R(3, 0)	201565.503	-0.008	0.02	6.7235015
R(3, 1)	201561.379	0.009	0.02	6.7233639
R(3, 2)	201548.956	0.019	0.02	6.7229495
R(3, 3)	201528.204	0.019	0.02	6.7222573
R(4, 0)	251946.642	-0.006	0.03	8.4040354
R(4, 1)	251941.470	-0.004	0.03	8.4038628
R(4, 2)	251925.939	-0.003	0.03	8.4033448
R(4, 3)	251900.037	0.020	0.03	8.4024808
R(4, 4)	251863.666	0.025	0.03	8.4012676
R(5, 0)	302320.972	0.016	0.03	10.0843421
R(5, 1)	302314.781	0.029	0.03	10.0841356
R(5, 2)	302296.124	-0.001	0.03	10.0835133
R(5, 3)	302265.047	0.010	0.03	10.0824767
R(5, 4)	302221.455	0.039	0.03	10.0810226
R(5, 5)	302165.191	0.033	0.03	10.0791459
R(8, 2)	453352.105	0.024	0.05	15.1221985
R(8, 3)	453305.597	0.019	0.05	15.1206471
R(8, 5)	453156.203	0.008	0.05	15.1156639
R(9, 0)	503722.539	0.007	0.05	16.8023753
R(9, 1)	503712.198	-0.033	0.05	16.8020304
R(9, 2)	503681.307	0.000	0.05	16.8009999
R(9, 3)	503629.679	-0.017	0.05	16.7992778
R(9, 4)	503557.301	0.012	0.05	16.7968635
R(9, 5)	503463.887	-0.030	0.05	16.7937476
R(9, 6)	503349.319	-0.026	0.05	16.7899260
R(9, 7)	503213.253	-0.002	0.05	16.7853873
R(9, 8)	503055.256	0.032	0.05	16.7801171
R(9, 9)	502874.769	0.062	0.05	16.7740967
R(10, 0)	554042.101	-0.061	0.06	18.4808552
R(10, 1)	554030.819	-0.025	0.06	18.4804789
R(10, 2)	553996.900	0.030	0.06	18.4793475
R(10, 3)	553940.177	0.007	0.06	18.4774554
R(10, 4)	553860.601	-0.024	0.06	18.4748010
R(10, 5)	553758.028	-0.027	0.06	18.4713796
R(10, 6)	553632.157	-0.047	0.06	18.4671810
R(10, 7)	553482.710	-0.017	0.06	18.4621959
R(10, 8)	553309.129	-0.037	0.06	18.4564059
R(10, 9)	553110.945	0.019	0.06	18.4497952
R(11, 0)	604346.712	-0.029	0.06	20.1588364
R(11, 1)	604334.395	-0.016	0.06	20.1584256
R(11, 2)	604297.404	0.007	0.06	20.1571917
R(11, 3)	604235.623	-0.005	0.06	20.1551309
R(11, 4)	604148.984	0.010	0.06	20.1522409
R(11, 5)	604037.199	-0.044	0.06	20.1485122
R(11, 6)	603900.127	-0.035	0.06	20.1439399
R(11, 7)	603737.328	-0.031	0.06	20.1385096
R(11, 8)	603548.294	-0.047	0.06	20.1322041
R(11, 9)	603332.499	0.029	0.06	20.1250059
R(12, 0)	654634.906	0.011	0.07	21.8362700
R(12, 1)	654621.556	-0.001	0.07	21.8358247
R(12, 2)	654581.497	-0.020	0.07	21.8344885
R(12, 3)	654514.701	0.003	0.07	21.8322604
R(12, 4)	654420.951	-0.014	0.07	21.8291332
R(12, 5)	654300.082	-0.032	0.07	21.8251015
R(12, 7)	653975.688	-0.102	0.07	21.8142809

[a] Observed minus calculated frequency in MHz. The parameters for the calculation are in the $v_3 = 1$ column of Table VI.

[b] Estimated uncertainty in the observed frequency in MHz.

[c] Observed frequency in cm^{-1}.

TABLE V

Sources of Data for Fits of the $v_3 = 0$, 1, and 2 States of $^{12}CH_3F$

Experiment	Source	Transitions	Uncert.[a]
IR-MW Sideband Laser	This work, Tables I and II.	High and low J,K; P,Q,R, $v_3 = 1, 2$.	1.0-3.0 MHz
	Ref. 11, Table I	High J,K; Q,R.	10.0 MHz
		Low J; P,R.	10.0 MHz
IR-MW Two-Photon	Ref. 4, Table I	Low J; P,Q,R.	6.0 MHz
IR Laser Stark	Ref. 2, Tables III and V.	Low J; P,Q,R. $v_3 = 1, 2$.	6.0 MHz
IR Laser Stark Lamb Dips	Ref. 2, Table III	Q(1,1), Q(2,2).	2.0 MHz
IR-RF Two-Photon	Ref. 2, Table III	Q(12,2).	2.0 MHz
	Ref. 3, Table III	Q(12,3).	1.0 MHz
Waveguide Laser	Ref. 24, Table I	Q(12,1), Q(12,2).	0.5 MHz
Diode Laser	Ref. 24, Table I	High J,K; Q, P(1,0).	10.0 MHz
	Ref. 5, Table 1	High J,K; P, R.	30.0 MHz
FIR Emission	Ref. 25, Table I	High J, pure rot., $v_3 = 0$ and 1.	5.0 MHz
mm Wave Lamb Dips	Ref. 16, Table 2	R(1,K), R(2,K), R(3,K), pure rot., $v_3 = 0$.	0.01 MHz
mm Wave	This work, Tables III and IV	High and low J; R, pure rot., $v_3 = 0$, 1.	0.02 to 0.09 MHz
	Ref. 17, Table I	R(4,K), pure rot., $v_3 = 0$.	0.1 MHz
	Ref. 18, Table VI	R(0,0), pure rot., $v_3 = 1$.	0.1 MHz
	Ref. 19, Table I	R(1,K), pure rot., $v_3 = 1$.	0.5 MHz
	Ref. 20, Table II	High and low J; R, pure rot., $v_3 = 0$.	0.05 to 0.12 MHz

[a]Uncertainty assumed in least squares fits.

of spectra to rather high J and K was comparable for fits that include explicit consideration of the Coriolis coupling and those that ignore it. Consequently, in the absence of better constants for the $v_6 = 1$ and higher states, it is better for most purposes to ignore the resonance.

IV. RESULTS

The frequencies of the vibration–rotation transitions observed in this work are given in Table I for the ν_3 fundamental band and in Table II for the $2\nu_3 \leftarrow \nu_3$ hot band. The frequencies of the rotational transitions observed in this work are given in Table III for the ground vibrational state and in Table IV for the $v_3 = 1$ state. The sources of previously reported experimental data that are included in the file of frequencies used in the least-squares fitting are summarized in Table V.

The frequencies in Tables I–IV together with those indicated in Table V have been used for a number of least-squares fits to energy levels calculated by means of Eq. (1).

TABLE VI

Vibration–Rotation Parameters for $^{12}CH_3F$

Parameter[a]	$v_3 = 0$[b]	$v_3 = 1$[b]	$v_3 = 2$[c]
E_v /GHz	0.0000[d]	31436.5561(3)	62398.208(1)
B_v /MHZ	25536.1499(6)	25197.5092(10)	24870.982(39)
$\Delta(A_v-B_v)$ /MHz	0.0000	44.3531(199)	81.301(105)
D_J /kHz	60.2330(36)	56.8788(59)	53.449(355)
D_{JK} /kHz	439.5743(312)	518.0831(492)	576.153(1014)
ΔD_K /kHz	0.0000	-94.0155(3047)	-169.646(2996)
H_J /Hz	-0.0218(68)	-0.2350(122)	-6.671(1107)
H_{JK} /Hz	1.7518(758)	15.9461(1278)	57.665(5245)
H_{KJ} /Hz	21.6679(1921)	-92.3407(6813)	-207.750(19286)
ΔH_K /Hz	0.0000	106.4444(16788)	172.750(36853)
L_J /mHz	0.0000[d]	0.0629(60)	8.384(1512)
L_{JJJK} /mHz	0.0000[d]	-2.8698(747)	-46.501(14416)
L_{JJKK} /mHz	0.0000[d]	41.2301(4777)	106.803(47568)
L_{JKKK} /mHz	0.0000[d]	-237.2909(18751)	-238.590(54249)
ΔL_K /mHz	0.0000	155.0075(31485)	142.613(99366)

[a] Vibration-rotation parameter. $\Delta P = P(v_3) - P(v_3=0)$.

[b] Obtained from fit of frequencies indicated in Tables I-IV and listed in Table V. Number in parentheses is one standard error in units of last digit in the parameter.

[c] It should be noted that the parameters for $v_3=2$ are given to one less significant figure than the parameters for $v_3=0$ and 1.

[d] Constrained to zero in the least squares fit.

TABLE VII

Comparison of Ground State Rotational Constants of $^{12}CH_3F$

Parameter	This Work[a]	This work[b]	Arimondo[c]	Boucher[d]
B_o /MHZ	25536.1499(6)	25536.1490(3)	25536.1492(2)	25536.14951(25)
D_J /kHz	60.2330(36)	60.2250(34)	60.207(8)	60.2186(70)
D_{JK} /kHz	439.5743(312)	439.6323(141)	439.62(3)	439.602(43)
H_J /Hz	-0.0218(68)	-0.0385(85)	-0.026(10)	-0.058(18)
H_{JK} /Hz	1.7518(758)	1.9257(408)	0.95(37)	1.81(13)
H_{KJ} /Hz	21.6679(1921)	21.5915(706)	26.2(34)	21.53(70)

[a] Obtained from fit of frequencies listed in Tables I-IV and those indicated in Table V.

[b] Obtained from fit of the frequencies in Table III.

[c] Obtained from Table 3 (Column 2) in Ref. 5.

[d] Obtained from Table I (MW data only) in Ref. 20.

TABLE VIII

Vibrational Dependence of Vibration–Rotation Parameters for $^{12}CH_3F$

P(v)[a]	P(0)[b]	c_1[b]	c_2[b]
E_v /GHz	0.000	ν_3 = 31674.008(1)	x_{33} = -237.452(1)
B_v /MHz	25536.150(1)	$-\alpha_3^B$ = -344.697(19)	6.057(19)
ΔA_v /MHz	0.000	$-\alpha_3^A$ = -296.642(69)	2.354(60)
D_J /kHz	60.233(4)	-3.316(178)	-0.038(178)
D_{JK} /kHz	439.574(31)	88.728(519)	-10.219(510)
ΔD_K /kHz	0.000	-103.208(1617)	9.192(1529)

[a]Vibration-rotation parameter. $P(v) = P(0) + c_1 v + c_2 v^2$. P(0), c_1, and c_2 were derived from the parameters in Table IV.

[b]Uncertainties in parentheses, in units of the last digit in the parameter, were propagated from one standard error in the parameters.

TABLE IX

Coincidences between Calculated Frequencies for the ν_3 Band of $^{12}CH_3F$ and CO_2 Laser Frequencies

Trans.[a]	Frequency[b]	$\nu_0-\nu_L$[c]	Laser[d]		
P(27,11)	29828909.0	-17.1	$^{13}C^{16}O_2$	BAND II	P(26)
Q(6, 4)	31423019.9	-87.6	$^{12}C^{16}O^{18}O$	BAND II	P(30)
Q(11, 1)	31391948.0	87.1	$^{13}C^{16}O_2$	BAND II	R(48)
Q(12, 1)	31383841.7	-58.9	$^{12}C^{16}O_2$	BAND II	P(20)
Q(12, 2)	31383940.1	39.6	$^{12}C^{16}O_2$	BAND II	P(20)
Q(13,13)	31382754.9	60.4	$^{13}C^{16}O_2$	BAND II	R(32)
Q(14, 2)	31365702.8	-54.3	$^{13}C^{16}O_2$	BAND II	R(46)
Q(14, 3)	31365849.8	92.7	$^{13}C^{16}O_2$	BAND II	R(46)
Q(15,15)	31365845.0	86.4	$^{13}C^{16}O_2$	BAND II	R(46)
Q(21,15)	31286137.6	-28.4	$^{12}C^{16}O^{18}O$	BAND II	P(35)
Q(28, 3)	31163602.8	93.3	$^{12}C^{18}O_2$	BAND II	P(54)
Q(28, 4)	31163526.6	17.0	$^{12}C^{18}O_2$	BAND II	P(54)
Q(28, 5)	31163432.1	-77.5	$^{12}C^{18}O_2$	BAND II	P(54)
Q(33, 8)	31058741.4	-78.2	$^{12}C^{16}O^{18}O$	BAND II	P(43)
Q(34,15)	31029723.8	23.8	$^{12}C^{16}O^{18}O$	BAND II	P(44)
Q(38, 2)	30941471.5	48.9	$^{12}C^{16}O^{18}O$	BAND II	P(47)
Q(39, 8)	30912521.1	39.2	$^{13}C^{16}O_2$	BAND II	R(18)
R(10, 3)	31953615.9	17.1	$^{12}C^{16}O^{18}O$	BAND II	P(9)
R(11, 9)	31998587.9	-26.1	$^{12}C^{18}O_2$	BAND II	P(22)
R(11,11)	32000205.2	-78.8	$^{12}C^{16}O^{18}O$	BAND II	P(7)
R(26,15)	32550672.7	25.4	$^{12}C^{18}O_2$	BAND II	R(2)
R(31, 4)	32708073.7	-22.1	$^{12}C^{18}O_2$	BAND II	R(10)
R(34, 3)	32791507.1	37.9	$^{12}C^{16}O^{18}O$	BAND II	R(32)
R(35,12)	32807743.3	-47.3	$^{12}C^{16}O^{18}O$	BAND II	R(33)

[a]Transition in the ν_3 band of $^{12}CH_3F$; $J \leq 40$, $K \leq 15$.

[b]Frequency of ν_3 band transition in MHz.

[c]Frequency of ν_3 band transition minus laser frequency in MHz. Laser frequencies calculated from constants in Refs. 32, 33, and 34.

[d]Identification of CO_2 or N_2O laser. Band I is 10 μm band; Band II is 9 μm band.

The vibration–rotation parameters obtained for a fit in which all of the parameters for $N \leqq 3$ for $v_3 = 0$ and $N \leqq 4$ for $v_3 = 1$ and 2 were varied are given in Table VI. These parameters were used to calculate the values for the comparison of observed and calculated frequencies in Tables I–IV. In a second fitting parameters were determined by constraining the ground state constants to those reported by Arimondo *et al.* (*5*), which were obtained from a fitting that included Graner's ground state combination differences (*21*). The constants from this fitting are in close agreement with those in Table VI. The reason for this may be seen in Table VII where the parameters for the ground state obtained from the fit in Table VI are compared to the corresponding parameters obtained by fitting only the data in Table III, and to the constants reported by Arimondo *et al.* (*5*) and Boucher *et al.* (*20*). The ground state parameters obtained from our full fitting (Table VI) are in very good agreement with those obtained from a variety of purely ground state data.

The vibrational dependence (Eq. (2)) of the constants calculated from the parameters in Table VI are shown inTable VIII, where the more usual notation for some of the parameters is indicated.

In Tables IX and X the calculated (parameters in Table VI) vibration–rotation frequencies for the ν_3 ($J \leqq 40, K \leqq 15$) and $2\nu_3 \leftarrow \nu_3$ ($J \leqq 25, K \leqq 12$) bands, respectively,

TABLE X

Coincidences between Calculated Frequencies for the $2\nu_3 \leftarrow \nu_3$ Band of $^{12}CH_3F$ and CO_2 Laser Frequencies

Trans.[a]	Frequency[b]	$\nu_0-\nu_L$[c]	Laser[d]	
P(22, 0)	29705011.1	-95.3	$^{12}C^{16}O^{18}O$ BAND I	R(40)
P(22, 1)	29705048.0	-58.3	$^{12}C^{16}O^{18}O$ BAND I	R(40)
P(22, 2)	29705159.4	53.0	$^{12}C^{16}O^{18}O$ BAND I	R(40)
P(21, 7)	29770679.7	11.6	$^{13}C^{16}O_2$ BAND II	P(28)
P(20, 6)	29833266.8	-67.1	$^{12}C^{16}O^{18}O$ BAND I	R(50)
Q(10, 6)	30926970.0	-23.0	$^{13}C^{18}O_2$ BAND II	R(6)
Q(16, 5)	30873622.0	-58.4	$^{13}C^{16}O_2$ BAND II	R(16)
Q(17, 1)	30861966.1	68.6	$^{12}C^{16}O_2$ BAND II	P(38)
Q(18, 8)	30851728.0	-37.0	$^{12}C^{16}O^{18}O$ BAND II	P(50)
Q(25,12)	30752051.6	-7.0	$^{13}C^{16}O_2$ BAND II	R(10)
R(7, 3)	31341429.0	5.8	$^{12}C^{16}O^{18}O$ BAND II	P(33)
R(10, 0)	31472640.0	-97.0	$^{13}C^{18}O_2$ BAND II	R(38)
R(10, 1)	31472658.6	-78.4	$^{13}C^{18}O_2$ BAND II	R(38)
R(10, 2)	31472715.3	-21.7	$^{13}C^{18}O_2$ BAND II	R(38)
R(10, 3)	31472812.2	75.2	$^{13}C^{18}O_2$ BAND II	R(38)
R(12, 4)	31557183.7	-54.3	$^{13}C^{18}O_2$ BAND II	R(44)
R(12, 5)	31557332.0	94.0	$^{13}C^{18}O_2$ BAND II	R(44)
R(13, 6)	31598591.2	35.1	$^{12}C^{18}O_2$ BAND II	P(38)

[a] Transition in the $2\nu_3 \leftarrow \nu_3$ band of $^{12}CH_3F$; $J \leq 25$, $K \leq 12$.

[b] Frequency of $2\nu_3 \leftarrow \nu_3$ band transition in MHz.

[c] Frequency of $2\nu_3 \leftarrow \nu_3$ band transition minus laser frequency in MHz. Laser frequencies calculated from constants in Refs. 32, 33, and 34.

[d] Identification of CO_2 or N_2O laser. Band I is 10 μm band; Band II is 9 μm band.

that lie within 100 MHz of a CO_2 laser frequency are shown together with the calculated offset. The CO_2 parameters for this calculation were taken from Refs. (*32–34*).

V. DISCUSSION

As indicated in the Introduction it was not possible with the parameters previously available for the ν_3 band to compute the frequencies for $J \sim 20$ to an accuracy of 10–20 MHz. This situation, which appeared to be mainly the result of an insufficient number of precise *P*-band frequencies, has been remedied. It should now be possible to compute the frequencies for $J \leqslant 30$, $K \leqslant 15$ for the ν_3 band and $J \leqslant 20$, $K \leqslant 10$ for the $2\nu_3 \leftarrow \nu_3$ band to an accuracy of $\sim$5 MHz. In addition, it should be possible to calculate all of the rotational frequencies for $J \leqslant 20$ for $v_3 = 0$ and $J \leqslant 14$ for $v_3 = 1$ to $\sim$80 kHz. In all cases the uncertainties rise rapidly with J and K and are much smaller for low J.

The overall standard deviation for an observation of unit weight for the 668 frequencies included in the full fitting was 1.3 MHz, which could be the result of a 30% underestimation of the experimental uncertainties, an inadequacy of the model used for the calculation, or some combination of these two effects. We believe that the discrepancy is mainly the result of model error. One indication that this might be so is that inclusion of L constants ($N = 4$ in Eq. (1)) for the ground state rotational levels does not improve the fit significantly. By contrast, L constants are essential for $v_3 = 1$ and 2. This is probably a result of an attempt by the power series expansion (Eq. (1)) to account for the Coriolis coupling to the ν_6 levels.

RECEIVED: September 26, 1986

REFERENCES

1. S. K. LEE, R. H. SCHWENDEMAN, AND G. MAGERL, *J. Mol. Spectrosc.* **117,** 416–434 (1986).
2. S. M. FREUND, G. DUXBURY, M. ROMHELD, J. T. TIEDJE, AND T. OKA, *J. Mol. Spectrosc.* **52,** 38–57 (1974); M. ROMHELD, Ph.D. thesis, University of Ulm, 1979.
3. E. ARIMONDO AND M. INGUSCIO, *J. Mol. Spectrosc.* **75,** 81–86 (1979).
4. P. SHOJA-CHAGHERVAND AND R. H. SCHWENDEMAN, *J. Mol. Spectrosc.* **98,** 27–40 (1983).
5. E. ARIMONDO, M. I. SCHISANO, P. B. DAVIES, AND P. A. HAMILTON, *Infrared Phys.* **25,** 209–213 (1985).
6. G. MAGERL, W. SCHUPITA, AND E. BONEK, *IEEE J. Quantum Electron.* **QE-18,** 1214–1220 (1982).
7. G. MAGERL, E. BONEK, AND W. A. KREINER, *Chem. Phys. Lett.* **52,** 473–476 (1977).
8. G. MAGERL, W. A. KREINER, B. FURCH, AND E. BONEK, *Acta Phys. Austriaca Suppl.* **20,** 167–179 (1979).
9. W. A. KREINER, G. MAGERL, B. FURCH, AND E. BONEK, *J. Chem. Phys.* **70,** 5015–5020 (1979).
10. G. MAGERL, W. SCHUPITA, E. BONEK, AND W. A. KREINER, *J. Chem. Phys.* **72,** 395–398 (1980).
11. G. MAGERL, W. SCHUPITA, E. BONEK, AND W. A. KREINER, *J. Mol. Spectrosc.* **83,** 431–439 (1980).
12. G. MAGERL, J. M. FRYE, W. A. KREINER, AND T. OKA, *Appl. Phys. Lett.* **42,** 656–658 (1983).
13. G. MAGERL, W. SCHUPITA, J. M. FRYE, W. A. KREINER, AND T. OKA, *J. Mol. Spectrosc.* **107,** 72–83 (1984).
14. H. SASADA, R. H. SCHWENDEMAN, G. MAGERL, R. L. POYNTER, AND J. M. MARGOLIS, *J. Mol. Spectrosc.* **117,** 317–330 (1986).
15. H. SASADA AND R. H. SCHWENDEMAN, *J. Mol. Spectrosc.* **117,** 331–341 (1986).
16. R. S. WINTON AND W. GORDY, *Phys. Lett.* **32A,** 219–220 (1970).
17. T. E. SULLIVAN AND L. FRENKEL, *J. Mol. Spectrosc.* **39,** 185–201 (1971).
18. T. TANAKA AND E. HIROTA, *J. Mol. Spectrosc.* **54,** 437–446 (1975).

19. E. HIROTA, T. TANAKA, AND S. SAITO, *J. Mol. Spectrosc.* **63,** 478–484 (1976).
20. D. BOUCHER, J. BURIE, R. BOCQUET, AND J. DEMAISON, *J. Mol. Spectrosc.* **116,** 256–258 (1986).
21. G. GRANER, *Mol. Phys.* **31,** 1833–1843 (1976).
22. S. M. FREUND, M. ROMHELD, AND T. OKA, *Phys. Rev. Lett.* **35,** 1497–1500 (1975).
23. J. P. SATTLER AND G. J. SIMONIS, *IEEE J. Quantum Electron.* **QE-13,** 461–465 (1977).
24. F. HERLEMONT, M. LYSZAK, J. LEMAIRE, AND J. DEMAISON, *Z. Naturforsch.* **36a,** 944–947 (1981).
25. T. Y. CHANG AND T. J. BRIDGES, *Opt. Commun.* **1,** 423–426 (1970).
26. T. Y. CHANG AND J. D. MCGEE, *Appl. Phys. Lett.* **19,** 103–105 (1971).
27. E. BAVA, A. DEMARCHI, A. GODONE, R. BENEDETTI, M. INGUSCIO, P. MINGUZZI, F. STRUMIA, AND M. TONELLI, *Opt. Commun.* **21,** 46–48 (1977).
28. H. E. RADFORD, F. R. PETERSON, D. A. JENNINGS, AND J. A. MUCHA, *IEEE J. Quantum Electron.* **QE-13,** 92–94 (1977).
29. P. HELMINGER, J. K. MESSER, AND F. C. DE LUCIA, *Appl. Phys. Lett.* **42,** 309–310 (1983).
30. W. C. KING AND W. GORDY, *Phys. Rev.* **93,** 407–412 (1954).
31. T. Y. CHANG, *in* "Reviews of Infrared and Millimeter Waves" (K. J. Button *et al.,* Eds.), Vol. 2, pp. 1–28, Plenum, New York, 1984.
32. F. R. PETERSEN, E. C. BEATY, AND C. R. POLLOCK, *J. Mol. Spectrosc.* **102,** 112–122 (1983).
33. C. FREED, L. C. BRADLEY, AND R. G. O'DONNELL, *IEEE J. Quantum Electron.* **QE-16,** 1195–1206 (1980).
34. B. G. WHITFORD, K. J. SIEMSEN, H. D. RICCIUS, AND G. R. HANES, *Opt. Commun.* **14,** 70–74 (1975).